Journal of Materials Chemistry A

ROYAL SOCIETY OF CHEMISTRY

PAPER

View Article Online
View Journal | View Issue

Cite this: J. Mater. Chem. A, 2023, 11, 9840

Fused polycyclic lactam-based π-conjugated polymers for efficient nonfullerene organic solar cells†

Narumi Sato,[a] Sunbin Hwang,[b] Yuichi Tsuchii[a] and Takuma Yasuda *[ab]

Received 23rd February 2023
Accepted 20th April 2023

DOI: 10.1039/d3ta01127e

rsc.li/materials-a

The development of high-performance wide-bandgap polymers has attracted significant attention in recent non-fullerene organic solar cells (NF-OSCs) research, as the expansion of the options of polymer donors that are appropriately matched with nonfullerene acceptors can lead to the further improvement of photovoltaic properties. In this study, two wide-bandgap π-conjugated polymers, namely, **P(TPTI-BDT)** and **P(2DTP-BDT)**, based on fused pentacyclic bis-lactam and dimeric bis-lactam units, were prepared and used as the donor materials for NF-OSCs with **IT-4F** as the acceptor. The NF-OSCs based on the **P(TPTI-BDT):IT-4F** blends outperformed the corresponding **P(2DTP-BDT):IT-4F**-based devices, achieving high power conversion efficiencies of up to 11.7% without processing additives or post-treatments. Further investigation of the thin-film morphologies using X-ray diffraction and transmission electron microscopy revealed that both **P(TPTI-BDT)** and **P(2DTP-BDT)** adopted preferential face-on molecular orientations and formed finely nano-segregated bulk-heterojunction morphologies when blended with **IT-4F**.

Introduction

Organic solar cells (OSCs) have gained continuous research interest from both industry and academia due to their unique advantages, *e.g.*, lightweight, flexibility, transparency, and large-area manufacturing *via* solution processes.[1] The last few years have witnessed an abrupt increase in the power conversion efficiency (PCE) of OSCs. State-of-the-art single-junction OSCs have achieved PCEs exceeding 18%,[2–5] thus demonstrating the significant potential for practical applications. Such PCE improvements are mainly due to the emergence of advanced photovoltaic materials, especially nonfullerene acceptors (NFAs) based on π-extended fused-ring structures.[6] NFAs demonstrate inherent advantages such as (i) stronger absorptions covering wider spectral ranges (including the near-infrared region), (ii) tunability of energy levels, (iii) higher charge generation efficiencies with small driving forces, and (iv) improved film-forming capacity when compared with traditional fullerene acceptors. As reported by Zou *et al.*[7] in 2019, Y6 is currently a high-performing benchmark NFA, and the most recent OSCs that achieve high PCEs (>18%) are dependent on the use of Y-series NFAs.[2–5] For bulk-heterojunction (BHJ) OSCs, NFAs and donor materials play equally critical roles in determining the photovoltaic function. However, the options of effective donor materials for nonfullerene OSCs (NF-OSCs) are inadequate and limited to several polymers such as PM6 (PBDB-TF),[2,8] D18,[3] PBQx-TF,[4] and PTQ10.[5,9] Thus, it is necessary to further expand the material space and explore effective wide-bandgap polymer donors that are compatible with NFAs.

Aromatic lactams are extensively employed as basic structures in functional dyes and pigments, typified by diketopyrrolopyrrole (DPP)[10] and isoindigo (IID)[11] (Fig. 1). Moreover, they are utilized as electron-accepting (A) units in the design of alternating donor–acceptor (D–A) π-conjugated copolymers. In 2013, Ding *et al.* developed thieno[2′,3′:5,6]pyrido[3,4-*g*]thieno[3,2-*c*]isoquinoline-5,11(4*H*,10*H*)-dione (TPTI) featuring a fused pentacyclic π-system with two electron-withdrawing lactam (pyridone) moieties.[12] The D–A copolymer consisting of alternating thiophene and TPTI units demonstrated a PCE of 7.8% when blended with a fullerene acceptor, $PC_{71}BM$. Thereafter, several TPTI-based polymers were reported to serve as donor materials in OSCs.[13] However, the photovoltaic performances of TPTI-based polymers in NF-OSCs have not been extensively investigated. The development of new TPTI-based systems that

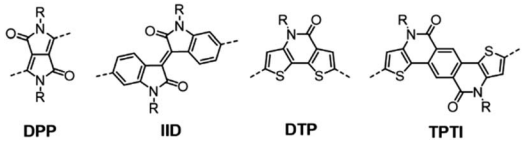

Fig. 1 Representative lactam-containing π-systems.

[a]Department of Applied Chemistry, Graduate School of Engineering, Kyushu University, Fukuoka, Japan. E-mail: yasuda@ifrc.kyushu-u.ac.jp

[b]Institute for Advanced Study, Kyushu University, Fukuoka, Japan

† Electronic supplementary information (ESI) available. See DOI: https://doi.org/10.1039/d3ta01127e

are appropriately suited for NF-OSCs is required. Recently, PCEs of nearly 10% were achieved for NF-OSCs using related dithieno [3,2-*b*:2′,3′-*d*]pyridin-5(4*H*)-one (DTP)-based polymers.[14,15] The use of simple lactam-based building units can potentially lead to the production of more efficient donor polymers and donor–acceptor pairs, thus further facilitating the development of efficient NF-OSCs.

In this study, we designed and synthesized TPTI- and DTP-based π-conjugated polymers, namely, **P(TPTI-BDT)** and **P(2DTP-BDT)** (Fig. 2a), coupled with a dialkylthienyl-substituted benzodithiophene (BDT) unit. Incorporating these bis-lactams into π-conjugated backbones is an attractive design strategy to increase the rigidity and planarity, and lower the reorganization energy; thereby facilitating the charge transport of the resulting polymers. The **P(TPTI-BDT)** and **P(2DTP-BDT)** backbones can retain high coplanarity (Fig. 2b), which is beneficial for the formation of crystalline molecular assemblies in the solid state. Moreover, the strong electron-withdrawing bis-lactam units can lower the HOMO and LUMO levels of the polymers, contributing to the enhancement of the open-circuit voltage (V_{oc}) of the OSCs. In combination with **IT-4F** as a common NFA,[16] NF-OSCs based on **P(TPTI-BDT)** and **P(2DTP-BDT)** achieved adequately high PCEs of 11.7% and 9.2%, respectively, without processing additives or additional treatments.

Results and discussion

P(TPTI-BDT) and **P(2DTP-BDT)** were synthesized *via* polycondensation using Migita–Kosugi–Stille cross-coupling reactions between dibromo-TPTI or -2DTP and distannyl-BDT monomers, wherein a $Pd_2(dba)_3$ catalyst and P(*o*-tol)$_3$ ligand were used (see ESI† for details). The resulting polymers were purified by sequential Soxhlet extraction using methanol, acetone, hexane, and chloroform, and then reprecipitation in methanol. The number-average molecular weights (M_n) and polydispersity indices (PDIs) of **P(TPTI-BDT)** and **P(2DTP-BDT)** were 125 kDa/4.4 and 42 kDa/4.4, respectively. Despite their high M_n values and high backbone rigidity and coplanarity, both polymers exhibited sufficiently high solubilities in chloroform and chlorobenzene required for thin-film fabrication due to introduction of multiple branched alkyl chains.

As shown in Fig. 3a, the bandgap energies (E_g) of **P(TPTI-BDT)** and **P(2DTP-BDT)** as thin films were determined as 2.05 and 1.97 eV, respectively, by applying the Tauc method: $(\alpha h\nu)^n \propto (h\nu - E_g)$.[17] Here α is the absorption coefficient, $h\nu$ is the photon energy, and $n = 2$ for direct allowed transitions. The **P(TPTI-BDT)** film exhibited a slightly blue-shifted absorption peak (λ_{max} = 572 nm) when compared with that of the **P(2DTP-BDT)** film (λ_{max} = 591 nm), resulting in a slightly larger E_g. Moreover, both polymer films exhibited intense absorptions with large values of α (>10^5 cm^{-1}) in the range of 450–600 nm, which were complementary to that of **IT-4F** (ESI†). Thus, blend films with **IT-4F** can cover the entire visible spectral range, which is required for the realization of a high photocurrent in OSCs. To determine the HOMO energy levels (E_{HOMO} or ionization potentials), photoelectron yield spectroscopy was conducted on thin films. As depicted in Fig. 3b, **P(2DTP-BDT)** containing dimeric DTP units exhibited a slightly lower E_{HOMO} (−5.35 eV) than that of **P(TPTI-BDT)** with pentacyclic TPTI units (−5.30 eV). Given the above E_g values, the LUMO energy level (E_{LUMO} or electron affinity) of **P(2DTP-BDT)** was expected to decrease by ~0.1 eV relative to **P(TPTI-BDT)**. The optical data for **P(TPTI-BDT)** and **P(2DTP-BDT)** are listed in Table 1.

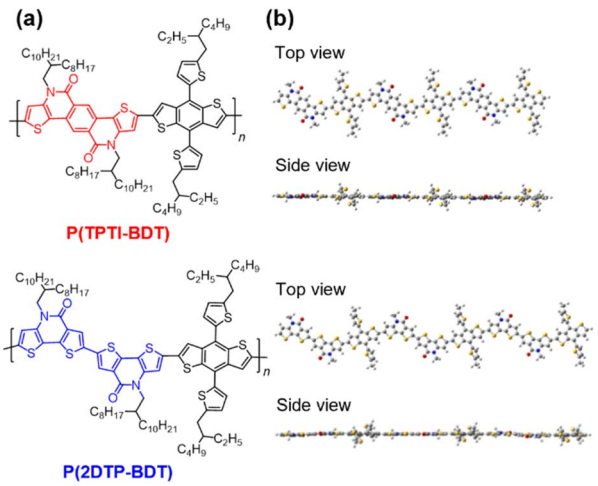

Fig. 2 (a) Chemical structures of P(TPTI-BDT) and P(2DTP-BDT), and (b) optimized molecular geometries for the respective trimeric segments calculated at the B3LYP/6-31G(d,p).

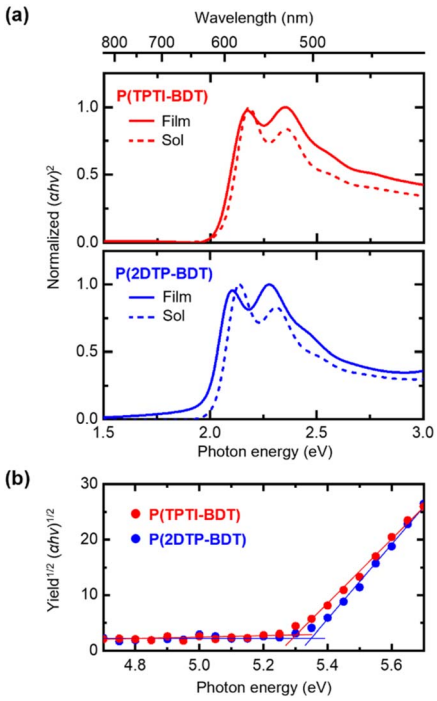

Fig. 3 (a) Tauc plots of $(\alpha h\nu)^2$ with respect to the photon energy ($h\nu$), as obtained from the optical absorption spectra of P(TPTI-BDT) and P(2DTP-BDT) in thin films (solid lines) and chloroform solutions (dashed lines). (b) Photoelectron yield spectra measured for the thin films of P(TPTI-BDT) and P(2DTP-BDT).

Table 1 Optical properties of the materials

Compound	λ_{max}[a] (nm) Sol[b]	Film[c]	E_{HOMO}[d] (eV)	E_{LUMO}[e] (eV)	E_g[f] (eV)
P(TPTI-BDT)	569	572	−5.30	−3.26	2.04
P(2DTP-BDT)	581	591	−5.35	−3.38	1.97
IT-4F	692	725	−5.87	−4.34	1.53

[a] Absorption peak wavelength. [b] Measured in chloroform solution (10^{-5} M) at 300 K. [c] Measured in a neat film spin-coated from chloroform solution onto a quartz substrate. [d] HOMO energy level determined by the photoelectron yield spectroscopy of neat film. [e] LUMO energy level calculated using $E_{LUMO} = E_{HOMO} + E_g$. [f] Optical bandgap derived from the Tauc plots for the neat film.

To evaluate the photovoltaic properties of **P(TPTI-BDT)** and **P(2DTP-BDT)**, NF-OSCs were fabricated using an inverted configuration of indium tin oxide (ITO, 100 nm)/ZnO (30 nm)/active layer (80–110 nm)/MoO_x (10 nm)/Ag (100 nm).[18] For all devices, each BHJ active layer, which consisted of a binary blend of **P(TPTI-BDT)** or **P(2DTP-BDT)** as the donor and **IT-4F** as the acceptor, was deposited by the spin-coating of their chloroform or chlorobenzene solutions without solvent additives. The weight ratios of the donor and acceptor in the blend films varied from 1 : 1 to 1 : 2.

The representative current density–voltage (J–V) curves and external quantum efficiency (EQE) spectra are shown in Fig. 4, and the relevant photovoltaic parameters are summarized in Table 2. For the **P(TPTI-BDT):IT-4F** binary systems, a PCE as high as 11.7% was achieved, along with a short-circuit current density (J_{sc}) of 19.6 mA cm^{-2}, V_{oc} of 0.86, and fill factor (FF) of 70%. It should be noted that high EQEs (photon-to-current conversion efficiencies) exceeding 80% over a wavelength range of 600–750 nm were achieved for the **P(TPTI-BDT):IT-4F**-based devices. The integrated current density from the EQE spectrum (J = 20.0 mA cm^{-2}) was consistent with the J_{sc} value obtained from the corresponding J–V curve. It is worth noting here that the as-spun BHJ active layers afforded a high PCE exceeding 11% without using any solvent additives or post-treatments. This significant feature allows for the development of high-efficiency OSCs using simpler processes.

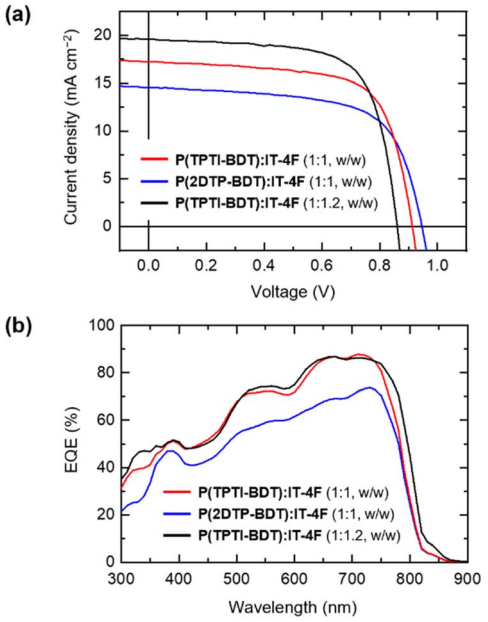

Fig. 4 (a) J–V curves measured under AM 1.5G 1-sun illumination (100 mW cm^{-2}) and (b) external quantum efficiency (EQE) spectra for the representative OSCs based on P(TPTI-BDT):IT-4F and P(2DTP-BDT):IT-4F BHJ blends.

The **P(2DTP-BDT):IT-4F**-based devices exhibited significantly high V_{oc} values (0.93–0.95 V), which can be attributed to the enlarged energy gap between the donor HOMO and acceptor LUMO levels. However, the **P(2DTP-BDT):IT-4F**-based devices exhibited lower PCEs (9.0–9.2%) when compared with the **P(TPTI-BDT):IT-4F**-based devices. This trend can be mainly attributed to the corresponding decrease in J_{sc}. Consistently, the EQEs of the **P(2DTP-BDT):IT-4F**-based devices decreased by approximately 10–20% over the entire visible region in comparison with the **P(TPTI-BDT):IT-4F**-based devices (Fig. 4b). It should be noted that PCEs decreased to only ~1% when combined with $PC_{71}BM$ instead of **IT-4F** (ESI†). The inferior performance for the fullerene-based devices can be attributed to the macroscopically phase-separated active layer morphology, which consists of large domains of the donor and acceptor agglomerates.

To gain insight into the molecular packing and orientation within the BHJ active layers, grazing-incidence X-ray diffraction (GIXD) measurements were performed. As can be seen from the two-dimensional (2D) GIXD patterns (Fig. 5a and b), for both pristine **P(TPTI-BDT)** and **P(2DTP-BDT)** films, a distinct diffraction corresponding to π–π stacking with a d-spacing of 3.7–3.8 Å (*i.e.*, (010) diffraction) was observed only along the out-of-plane q_z-axis direction, thus suggesting that **P(TPTI-BDT)** and **P(2DTP-BDT)** preferentially adopted a face-on orientation in the as-spun neat films. The observation of the (100) lamellar diffraction with a d-spacing of 22–23 Å in the in-plane q_{xy}-axis direction supports this trend. This dominant face-on orientation promoted efficient charge transport along the direction perpendicular to the substrate. Importantly, both polymers essentially retained their face-on orientations, even in blend films with **IT-4F** (Fig. 5c and d). However, the (100) lamellar diffraction along the out-of-plane direction intensified, indicating that face-on and edge-on polymer crystallites coexisted upon blending with **IT-4F**. Fig. 5e presents the pole figure analysis for the (010) π–π stacking diffractions in the two-dimensional (2D) GIXD patterns measured for the doped films, where the integrated intensities with respect to the azimuthal angle (χ) ranges of 45–135° (A_z) and 0–45° and 135–180° (A_{xy}) were defined as fractions of face-on and edge-on crystallites, respectively.[19] The A_z/A_{xy} ratios for the **P(TPTI-BDT):IT-4F** and **P(2DTP-BDT):IT-4F** blend films were calculated as 1.55 and 1.54, respectively, suggesting no significant difference in face-on molecular orientation.

Transmission electron microscopy (TEM) images of the blend films revealed distinct nanoscale phase segregation and interpenetrating network formation (Fig. 5f and g). Based on 2D

Table 2 Photovoltaic parameters for NF-OSCs

Active layer	D : A ratio (wt/wt)	t^a (nm)	J_{sc} (mA cm^{-2})	J^b (mA cm^{-2})	V_{oc} (V)	FF (%)	PCE^c (%)	$R_s{}^d$ (Ω cm^2)	$R_{sh}{}^e$ (Ω cm^2)
P(TPTI-BDT):IT-4F	1 : 1[f]	106	17.2	19.1	0.91	69	10.8	2.2	807
	1 : 2[f]	99	15.9	15.8	0.91	70	10.1	2.1	1050
	1 : 1.2[g]	109	19.6	20.0	0.86	70	11.7	1.5	988
P(2DTP-BDT):IT-4F	1 : 1[f]	82	14.6	15.9	0.95	65	9.0	2.5	736
	1 : 2[f]	85	14.5	15.8	0.93	68	9.2	2.5	886

[a] Active layer thickness determined using a profilometer. [b] Calculated by integrating the EQE spectra. [c] PCE = (J_{sc} × V_{oc} × FF)/P_0, where P_0 is the incident light intensity (100 mW cm^{-2}). [d] Series resistance. [e] Shunt resistance. [f] Using chloroform solvent. [g] Using chlorobenzene solvent.

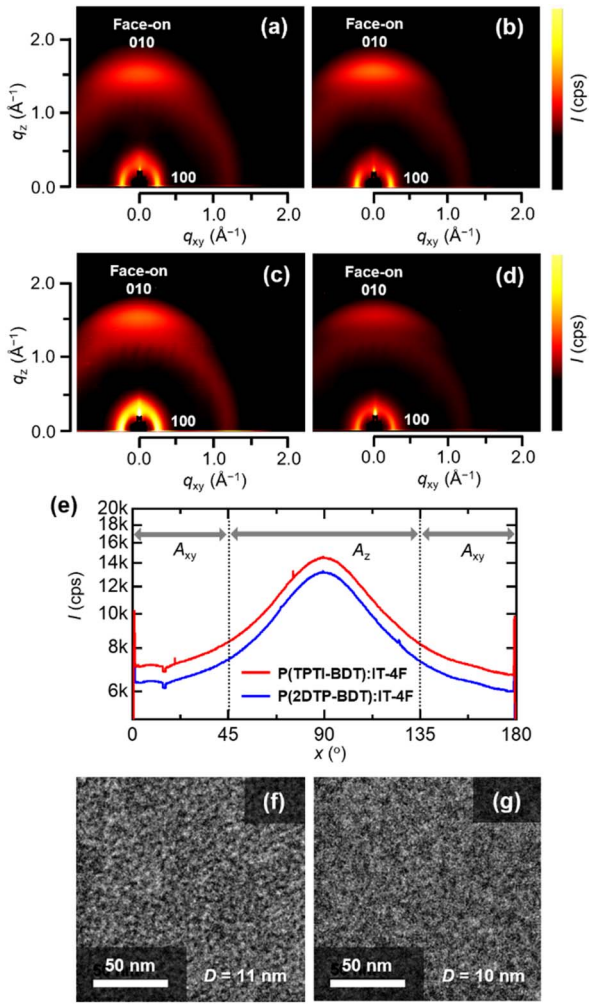

Fig. 5 Two-dimensional GIXD images for (a) **P(TPTI-BDT)** and (b) **P(2DTP-BDT)** neat films and (c) **P(TPTI-BDT):IT-4F** (1 : 1, w/w) and (d) **P(2DTP-BDT):IT-4F** (1 : 1, w/w) blend films. (e) Pole figures for the π−π stacking diffractions (d = 4.25–2.88 Å) in the blend films. TEM images of (f) **P(TPTI-BDT):IT-4F** (1 : 1, w/w) and (g) **P(2DTP-BDT):IT-4F** (1 : 1, w/w) blend films. The D values represent the average domain sizes calculated by 2D FFT analysis.

fast Fourier transform (FFT) analysis,[20] the average domain sizes (D), which correspond to the periodicity of the phase-segregated structures, were calculated as 11 and 10 nm for the **P(TPTI-BDT):IT-4F** and **P(2DTP-BDT):IT-4F** blend films, respectively. Appropriate domain sizes should be sufficiently small for exciton diffusion/dissociation in accordance with short exciton diffusion lengths (typically ~10 nm), and sufficiently large to secure charge transport channels. The interior morphologies spontaneously formed in these blend films meet these criteria, thus demonstrating excellent photovoltaic performances. The capacity to spontaneously form optimal morphologies without additives is a significant advantage of these polymers with respect to prospective applications.

Conclusions

In this paper, we reported two analogous wide-bandgap π-conjugated polymers, **P(TPTI-BDT)** and **P(2DTP-BDT)**, with different bis-lactam core structures. Although both polymers exhibited comparable optical properties, **P(TPTI-BDT)** with fused pentacyclic bis-lactam units was found to exhibit superior photovoltaic properties. When combined with **IT-4F** to fabricate NF-OSCs, the **P(TPTI-BDT)**-based devices achieved high PCEs of up to 11.7%, outperforming the **P(TPTI-BDT)**-based devices. The introduction of highly fused polycyclic frameworks can facilitate the formation of ordered nanostructures with preferential face-on orientations, even in blend films. Due to the lack of photoresponsivity in the near-infrared region, existing devices are less efficient than the state-of-the-art NF-OSCs incorporating Y-series NFAs. However, with excellent photoresponsive characteristics limited to the visible range with EQEs over 80%, the present material system can be used for both outdoor and indoor photovoltaic applications.[21] Further research will be conducted accordingly.

Author contributions

NS and TY designed experiments; NS synthesized the materials and performed spectroscopic measurements and device evaluations with the support of SH; SH and YT performed the structural analyses; TY and SH wrote the manuscript; and TY supervised the research project.

Conflicts of interest

There are no conflicts to declare.

Acknowledgements

This work was supported in part by Grant-in-Aid for the Adaptable and Seamless Technology Transfer Program through Target-driven R&D (A-STEP) from JST (Grant No. JPMJTR201B). The GIXD measurements were performed at the BL-40B2 beamline of SPring-8 with the approval of the Japan Synchrotron Radiation Research Institute (JASRI) (Proposal No. 2020A0825).

References

1 (*a*) G. Yu, J. Gao, J. C. Hummelen, F. Wudl and A. J. Heeger, *Science*, 1995, **270**, 1789–1791; (*b*) G. Li, R. Zhu and Y. Yang, *Nat. Photonics*, 2012, **6**, 153–161; (*c*) B. C. Thompson and J. M. J. Fréchet, *Angew. Chem., Int. Ed.*, 2007, **47**, 58–77; (*d*) Y. Huang, E. J. Kramer, A. J. Heeger and G. C. Bazan, *Chem. Rev.*, 2014, **114**, 7006–7043; (*e*) L. Lu, T. Zheng, Q. Wu, A. M. Schneider, D. Zhao and L. Yu, *Chem. Rev.*, 2015, **115**, 12666–12731.

2 (*a*) M. Zhang, L. Zhu, G. Zhou, T. Hao, C. Qiu, Z. Zhao, Q. Hu, B. W. Larson, H. Zhu, Z. Ma, Z. Tang, W. Feng, Y. Zhang, T. P. Russell and F. Liu, *Nat. Commun.*, 2021, **12**, 309; (*b*) C. Li, J. Zhou, J. Song, J. Xu, H. Zhang, X. Zhang, J. Guo, L. Zhu, D. Wei, G. Han, J. Min, Y. Zhang, Z. Xie, Y. Yi, H. Yan, F. Gao, F. Liu and Y. Sun, *Nat. Energy*, 2021, **6**, 605–613; (*c*) L. Zhang, S. Li, X. Xia, Y. Li, X. Lu, L. Zuo, M. Shi and H. Chen, *Adv. Mater.*, 2021, **33**, 2007231; (*d*) F. Liu, L. Zhou, W. Liu, Z. Zhou, Q. Yue, W. Zheng, R. Sun, W. Liu, S. Xu, H. Fan, L. Feng, Y. Yi, W. Zhang and X. Zhu, *Adv. Mater.*, 2021, **33**, 2100830; (*e*) Y. Cai, Y. Li, R. Wang, H. Wu, Z. Chen, J. Zhang, Z. Ma, X. Hao, Y. Zhao, C. Zhang, F. Huang and Y. Sun, *Adv. Mater.*, 2021, **33**, 2101733; (*f*) P. Bi, S. Zhang, Z. Chen, Y. Xu, Y. Cui, T. Zhang, J. Ren, J. Qin, L. Hong, X. Hao and J. Hou, *Joule*, 2021, **5**, 2408–2419; (*g*) L. Hong, H. Yao, Y. Cui, P. Bi, T. Zhang, Y. Cheng, Y. Zu, J. Qin, R. Yu, Z. Ge and J. Hou, *Adv. Mater.*, 2021, **33**, 2103091; (*h*) X. Xu, L. Yu, H. Meng, L. Dai, H. Yan, R. Li and Q. Peng, *Adv. Funct. Mater.*, 2022, **32**, 2108797; (*i*) L. Zhan, S. Li, Y. Li, R. Sun, J. Min, Z. Bi, W. Ma, Z. Chen, G. Zhou, H. Zhu, M. Shi, L. Zuo and H. Chen, *Joule*, 2022, **6**, 662–675; (*j*) L. Zhu, M. Zhang, J. Xu, C. Li, J. Yan, G. Zhou, W. Zhong, T. Hao, J. Song, X. Xue, Z. Zhou, R. Zeng, H. Zhu, C.-C. Chen, R. C. I. MacKenzie, Y. Zou, J. Nelson, Y. Zhang, Y. Sun and F. Liu, *Nat. Mater.*, 2022, **21**, 656–663; (*k*) C. He, Y. Pan, Y. Ouyang, Q. Shen, Y. Gao, K. Yan, J. Fang, Y. Chen, C.-Q. Ma, J. Min, C. Zhang, L. Zuo and H. Chen, *Energy Environ. Sci.*, 2022, **15**, 2537–2544.

3 (*a*) Q. Liu, Y. Jiang, K. Jin, J. Qin, J. Xu, W. Li, J. Xiong, J. Liu, Z. Xiao, K. Sun, S. Yang, X. Zhang and L. Ding, *Sci. Bull.*, 2020, **65**, 272–275; (*b*) Y. Wei, Z. Chen, G. Lu, N. Yu, C. Li, J. Gao, X. Gu, X. Hao, G. Lu, Z. Tang, J. Zhang, Z. Wei, X. Zhang and H. Huang, *Adv. Mater.*, 2022, **34**, 2204718.

4 Y. Cui, Y. Xu, H. Yao, P. Bi, L. Hong, J. Zhang, Y. Zu, T. Zhang, J. Qin, J. Ren, Z. Chen, C. He, X. Hao, Z. Wei and J. Hou, *Adv. Mater.*, 2021, **33**, 2102420.

5 (*a*) K. Chong, X. Xu, H. Meng, J. Xue, L. Yu, W. Ma and Q. Peng, *Adv. Mater.*, 2022, **34**, 2109516; (*b*) R. Ma, C. Yan, J. Yu, T. Liu, H. Liu, Y. Li, J. Chen, Z. Luo, B. Tang, X. Lu, G. Li and H. Yan, *ACS Energy Lett.*, 2022, **7**, 2547–2556.

6 For reviews, see:(*a*) C. Yan, S. Barlow, Z. Wang, H. Yan, A. K.-Y. Jen, S. R. Marder and X. Zhan, *Nat. Rev. Mater.*, 2018, **3**, 18003; (*b*) J. Hou, O. Inganäas, R. H. Friend and F. Gao, *Nat. Mater.*, 2018, **17**, 119–128; (*c*) G. Zhang, J. Zhao, P. C. Y. Chow, K. Jiang, J. Zhang, Z. Zhu, J. Zhang, F. Huang and H. Yan, *Chem. Rev.*, 2018, **118**, 3447–3507; (*d*) P. Cheng, G. Li, X. Zhan and Y. Yang, *Nat. Photonics*, 2018, **12**, 131–142; (*e*) A. Armin, W. Li, O. J. Sandberg, Z. Xiao, L. Ding, J. Nelson, D. Neher, K. Vandewal, S. Shoaee, T. Wang, H. Ade, T. Heumüller, C. Brabec and P. Meredith, *Adv. Energy Mater.*, 2021, **11**, 2003570.

7 J. Yuan, Y. Zhang, L. Zhou, G. Zhang, H.-L. Yip, T.-K. Lau, X. Lu, C. Zhu, H. Peng, P. A. Johnson, M. Leclerc, Y. Cao, J. Ulanski, Y. Li and Y. Zou, *Joule*, 2019, **3**, 1140–1151.

8 M. Zhang, X. Guo, W. Ma, H. Ade and J. Hou, *Adv. Mater.*, 2015, **27**, 4655–4660.

9 C. Sun, F. Pan, H. Bin, J. Zhang, L. Xue, B. Qiu, Z. Wei, Z.-G. Zhang and Y. Li, *Nat. Commun.*, 2018, **9**, 743.

10 (*a*) S. Qu and H. Tian, *Chem. Commun.*, 2012, **48**, 3039–3051; (*b*) C. Zhao, Y. Guo, Y. Zhang, N. Yan, S. You and W. Li, *J. Mater. Chem. A*, 2019, **7**, 10174–10199; (*c*) M. Kaur and D. H. Choi, *Chem. Soc. Rev.*, 2015, **44**, 58–77.

11 (*a*) R. Stalder, J. Mei, K. R. Graham, L. A. Estrada and J. R. Reynolds, *Chem. Mater.*, 2014, **26**, 664–678; (*b*) X. Wei, W. Zhang and G. Yu, *Adv. Funct. Mater.*, 2021, **31**, 2010979; (*c*) P. Deng and Q. Zhang, *Polym. Chem.*, 2014, **5**, 3298–3305.

12 J. Cao, Q. Liao, X. Du, J. Chen, Z. Xiao, Q. Zuo and L. Ding, *Energy Environ. Sci.*, 2013, **6**, 3224–3228.

13 (*a*) Q. Liao, J. Cao, Z. Xiao, J. Liao and L. Ding, *Phys. Chem. Chem. Phys.*, 2013, **15**, 19990–19993; (*b*) J. Cao, S. Chen, Z. Qi, Z. Xiao, J. Wang and L. Ding, *RSC Adv.*, 2014, **4**, 5085–5087; (*c*) C. Zuo, J. Cao and L. Ding, *Macromol. Rapid Commun.*, 2014, **35**, 1362–1366; (*d*) G. Feng, Y. Xu, C. Xiao, J. Zhang, X. Zhang, C. Li, Z. Wei, W. Hu, Z. Wang and W. Li, *Polym. Chem.*, 2016, **7**, 164–170; (*e*) H. J. Cho, Y. J. Kim, S. Chen, J. Lee, T. J. Shin, C. E. Park and C. Yang, *Nano Energy*, 2017, **39**, 229–237; (*f*) S. Chen, H. J. Cho, J. Lee, Y. Yang, Z.-G. Zhang, Y. Li and C. Yang, *Adv. Energy Mater.*, 2017, **7**, 1701125; (*g*) P. Gao, J. Tong, P. Guo, J. Li, N. Wang, C. Li, X. Ma, P. Zhang, C. Wang and Y. Xia, *J. Polym. Sci., Part A: Polym. Chem.*, 2018, **56**, 85–95.

14 (*a*) Y. Gao, D. Li, Z. Xiao, X. Qian, J. Yang, F. Liu, S. Yang and L. Ding, *Mater. Chem. Front.*, 2019, **3**, 339–402; (*b*) M. An, F. Xie, X. Geng, J. Zhang, J. Jiang, Z. Lei, D. He, Z. Xiao and L. Ding, *Adv. Energy Mater.*, 2017, **7**, 1602509.

15 Y. Tsuchii, T. Menda, S. Hwang and T. Yasuda, *Bull. Chem. Soc. Jpn.*, 2023, **96**, 90–94.

16 (*a*) W. Zhao, S. Li, H. Yao, S. Zhang, Y. Zhang, B. Yang and J. Jou, *J. Am. Chem. Soc.*, 2017, **139**, 7148–7151; (*b*) T. J. Aldrich, M. Matta, W. Zhu, S. M. Swick, C. L. Stern, G. C. Shatz, A. Facchetti, F. S. Melkonyan and T. J. Marks, *J. Am. Chem. Soc.*, 2019, **141**, 3274–3287.

17 J. Tauc, *Mater. Res. Bull.*, 1968, **3**, 37–46.

18 (*a*) W. Shin, T. Yasuda, Y. Hidaka, G. Watanabe, R. Arai, K. Nasu, T. Yamaguchi, W. Murakami, K. Makita and C. Adachi, *Adv. Energy Mater.*, 2014, **4**, 1400879; (*b*) H. Komiyama, T. To, S. Furukawa, Y. Hidaka, W. Shin, T. Ichikawa, R. Arai and T. Yasuda, *ACS Appl. Mater. Interfaces*, 2018, **10**, 11083–11093; (*c*) S. Furukawa, H. Komiyama, N. Aizawa and T. Yasuda, *ACS Appl. Mater. Interfaces*, 2018, **10**, 42756–42765; (*d*) R. Arai, S. Furukawa, Y. Hidaka, H. Komiyama and T. Yasuda, *ACS Appl. Mater. Interfaces*, 2019, **11**, 9259–9264; (*e*) S. Furukawa and T. Yasuda, *J. Mater. Chem. A*, 2019, **7**, 14806–14815.

19 (*a*) V. Vohra, K. Kawashima, T. Kakara, T. Koganezawa, I. Osaka, K. Takimiya and H. Murata, *Nat. Photonics*, 2015, **9**, 403–408; (*b*) P. Müller-Buschbaum, *Adv. Mater.*, 2014, **26**, 7692–7709; (*c*) J. Rivnay, S. C. B. Mannsfeld, C. E. Miller, A. Salleo and M. F. Toney, *Chem. Rev.*, 2012, **112**, 5488–5519.

20 (*a*) W. Ma, C. Yang and A. J. Heeger, *Adv. Mater.*, 2007, **19**, 1387–1390; (*b*) J. S. Moon, J. K. Lee, S. Cho, J. Byun and A. J. Heeger, *Nano Lett.*, 2009, **9**, 230–234.

21 S. Hwang and T. Yasuda, *Polym. J.*, 2023, **55**, 297–316.